

Influences of crystallographic orientations on deformation mechanism and grain refinement of Al single crystals subjected to one-pass equal-channel angular pressing

W.Z. Han *, Z.F. Zhang, S.D. Wu *, S.X. Li

Shenyang National Laboratory for Materials Science, Institute of Metal Research, Chinese Academy of Sciences, Shenyang 110016, China

Received 15 May 2007; received in revised form 30 June 2007; accepted 2 July 2007

Available online 20 August 2007

Abstract

The influences of crystallographic orientations on the evolution of dislocation structures and the refinement process of sub-grains in Al single crystals processed by one-pass equal-channel angular pressing (ECAP) were systematically investigated by means of scanning electron microscopy, electron backscatter diffraction and transmission electron microscopy. Three single crystals with different orientations, denoted as crystal I, crystal II and crystal III, were specially designed according to the shape of the ECAP die. For crystal I, its insert direction is parallel to $[1\ 1\ 0]$ and its extrusion direction is parallel to $[\bar{1}\ 1\ 1]$. For crystal II, the $(\bar{1}\ 1\ 1)$ plane is located parallel to the intersection plane of the ECAP die, and the $[1\ 1\ 0]$ direction is along the general shear direction on the intersection plane. For crystal III, the $(\bar{1}\ 1\ 1)$ plane is laid on the plane perpendicular to the intersection of the ECAP die, and the $[1\ 1\ 0]$ direction is vertical to the general shear direction. For crystal I, abundant cell block structures with multi-slip characters were formed, and they should be induced by four symmetric slip systems, while for crystal II, there are two sets of sub-grain structures with higher misorientation, making an angle of $\sim 70^\circ$, which can be attributed to the interactions of the two asymmetric primary slip planes, whereas for crystal III, only one set of ribbon structures was parallel to the traces of $(\bar{1}\ 1\ 1)$ with the lowest misorientation angle among the three single crystals, which should result from the homogeneous slip on the primary slip plane. The different microstructural features of the three single crystals provide clear experimental evidence that the microstructures and misorientation evolution are strongly affected by the crystallographic orientation or by the interaction between shear deformation imposed by the ECAP die and the intrinsic slip deformation of the single crystals. Based on the experimental results and the analysis of the ECAP deformation mechanism, a new possible deformation model is suggested for the crystalline materials subjected to ECAP.

© 2007 Published by Elsevier Ltd on behalf of Acta Materialia Inc.

Keywords: Equal-channel angular pressing (ECAP); Single crystal; Crystallographic orientation; Slip system; Shear deformation

1. Introduction

Recently, various techniques based on severe plastic deformation have been developed for substantially refining grains in metals and alloys in order to enhance their properties. For example, equal-channel angular pressing (ECAP), high pressure torsion (HPT) and surface mechanical attrition treatment (SMAT), etc. [1–11] have been

widely used for synthesizing ultrafine-grained materials and, accordingly, their mechanical strengths are remarkably improved. As a result, the understanding of the fundamental mechanism of strain-induced grain refinement is crucial not only for the theoretical requirement, but also for the technological development of the advanced engineering materials produced by severe plastic deformation (SPD) techniques.

ECAP as one of the major SPD methods has been widely used to fabricate ultrafine-grained materials for a decade [3,4,6–16]. The mechanism of grain refinement via ECAP has been extensively investigated in numerous mate-

* Corresponding authors. Tel.: +86 24 83978023.

E-mail addresses: wzhan@imr.ac.cn (W.Z. Han), shdwu@imr.ac.cn (S.D. Wu).

rials [12–16]. In view of potential industrial application and the scientific merit of ECAP, it is important to clarify the effect of crystallographic orientation on microstructural refinement in order to design an efficient manufacturing process or to understand the texture evolution during ECAP. However, only a few reports concern the effect of initial crystallographic orientation on the grain refinement process and texture evolution [17–19]. Recently, the deformation experiments of single crystals have been attempted in ECAP for a deeper insight into the influence of the processing route and crystallographic orientations on the grain refinement mechanism [20–23]. Fukuda et al. [20,21] investigated the microstructural evolution of an Al single crystal with known orientation during the process of ECAP. They found that the detailed experimental observations are fully consistent with the expectations from crystallographic considerations. Miyamoto et al. [22,23] processed a series of Cu single crystals by the ECAP technique. They reported that some single crystals with insert direction parallel to $[110]$ still remained as a single orientation after extrusion, while some others have two to three orientations. Those investigators have acquired some interesting results, but several questions still remain, i.e., (a) why some single crystals still remained as a single orientation after ECAP; (b) why the processed single crystal by Fukuda et al. [20] has large misorientations after ECAP, although it was designed to make one of the slip systems just meeting the macro-scale shear deformation of ECAP. Therefore, the microstructural evolutions of single crystals during ECAP still need further investigation.

The evolution of the microstructures during deformation of single crystals has been found to depend on the crystallographic orientation of the grains in which the microstructure develops [24,25]. The different microstructural features are closely related to the slip pattern, as has been deduced by applying Schmid factor analysis to derive the active slip systems [26]. Thereby, a link could be established between the microstructural characteristics and the macroscopic plastic behaviors. Therefore, in order fully to understand the microstructural evolution during ECAP for different single crystals, it is important to understand the macro-scale deformation mode of ECAP. In general, the large shear deformation in ECAP is always considered to occur along the intersection plane between the entrance and exit channels, and the intersection plane is just the shear deformation plane [27–29]. As a result, it is naturally expected to find a group of elongated structures within the ECAPed metals, which should be parallel to the intersection plane and make an angle of 45° with respect to the extrusion direction (ED) for the polycrystalline materials processed by the right angle ECAP die. However, many experimental results have proved that, after pressing for the first pass, a group of shear flow lines taking an angle of $\sim 27^\circ$ with respect to the ED were formed in the ECAPed metals [30–35]. It seems to be in contradiction to the macro-scale deformation model of ECAP and the corresponding experimental results. Therefore, the deformation mechanism of crystalline materials

during ECAP is, in fact, not yet well understood. Recently, some experimental results have demonstrated that it is more reasonable and easier to understand the deformation behavior during ECAP from the view of metal flow than the general simple shear theory [36], indicating that the direction perpendicular to the intersection plane is the most possible macro-scale shear direction. Previously, Segal [28] pointed out that there are two maximum shear stress directions during ECAP: one is along the intersection direction, and another is vertical to it. However, only very limited information is available on how the two maximum shear stresses affect the microstructures during extrusion.

In the present work, three specially oriented Al single crystals were designed, and then shear deformation by ECAP was applied and the microstructures formed were characterized by various techniques in order to reveal the two issues systematically. (i) How does the initial crystallographic orientation affect the refinement process of single crystals? (ii) And how does the deformation mode of ECAP determine the grain refinements of single crystals?

2. Experimental procedure

2.1. Experimental design

The present experiments were conducted using three different orientated single crystals of high-purity aluminum (99.999%) grown from the melting using the vertical Bridgeman method. The initial crystallographic orientations of the single crystal were determined using the electron backscatter diffraction (EBSD) method. In order to investigate the influence of orientations on the refinement process and the deformation mechanism during ECAP, the initial orientations of these single crystals were specially designed. Fig. 1 demonstrates the schematic of the ECAP die and the

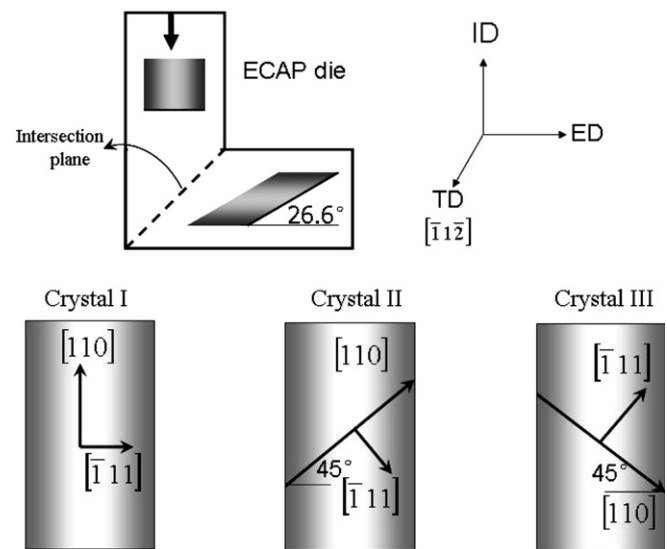


Fig. 1. Schematic illustration of the ECAP coordinates and the current experimental design (ID for insert direction, TD for transverse direction and ED for extrusion direction).

corresponding orientations of the three single crystals. These single crystals are named crystal I, crystal II and crystal III, respectively, as shown in Fig. 1. The insert direction (ID) of crystal I is parallel to $[110]$ and its ED is parallel to $[\bar{1}11]$. For crystal II, the $(\bar{1}11)$ is purposely located parallel to the intersection plane of the ECAP die and the $[110]$ is along the general shear direction on the intersection plane, as demonstrated in Fig. 1. For crystal III, the $(\bar{1}11)$ is perpendicular to the intersection plane of the ECAP die, while the $[110]$ is vertical to the general shear direction. It is worth pointing out that when a uniaxial compression along the direction of ID is applied, the stress state and deformation between crystals II and III will have no difference in nature. However, in the ECAP deformation, they may behave in quite a different manner.

2.2. The ECAP procedures

Samples of three Al single crystals with 40 mm long were cut according to the design, as shown in Fig. 1. Then these single crystals were extruded for only one pass by a right-angle ECAP die at room temperature with an extrusion rate of 5 mm min^{-1} and lubrication of MoS_2 . The cross-section of the work piece is 10 mm in diameter. Three orthogonal directions are defined as shown in Fig. 1, where the ID-ED plane is just the $(\bar{1}12)$ crystallographic plane for the three single crystals in the present experiment.

2.3. Microstructural characterization

After ECAP, the microstructural characterizations were performed using transmission electron microscopy (TEM; JEM-2000FXII) and scanning electron microscopy (SEM; Cambridge S-360 and LEO SUPRA 35-FEG-SEM). Thin foils for TEM and the samples for SEM were focused on the ID-ED plane in the center of the pressed rods. The prepared thin foils were then first mechanically ground to $\sim 50 \mu\text{m}$ thick and finally thinned by a twin-jet polishing method in a solution of 20% nitric acid and 80% carbinol in a voltage range of 8–10 V at room temperature. The samples for SEM and EBSD experiments were then mechanically ground using the abrasive paper and finally electro-polishing in a solution of 20% perchloric acid and 80% alcohol. The EBSD experiment was conducted on a LEO SUPRA 35-FEG-SEM with map step size of $0.8 \mu\text{m}$ and the image area was set at $500 \times 500 \mu\text{m}^2$.

3. Experimental results

3.1. Microstructures and misorientations observed by SEM and EBSD

Fig. 2 shows the SEM electron channeling contrast (SEM-ECC) images on the ID-ED plane of three single crystals after one-pass ECAP. It can be seen that the refinement results are totally different for the three single crystals due to the orientation differences. Crystal I is composed of

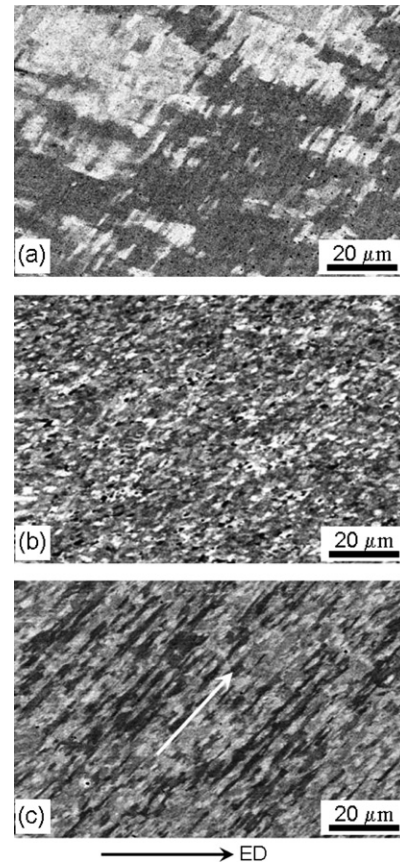


Fig. 2. Typical SEM-ECC micrographs of deformation microstructures of Al single crystals after one-pass ECAP: (a) crystal I; (b) crystal II; (c) crystal III in ID-ED.

relatively coarser microstructure than crystals II and III. The finest microstructure with almost equiaxed grains or sub-grains is achieved within crystal II. While the microstructure for crystal III only consists of a series of ribbons. One can find that those ribbon structures make an angle of $\sim 45^\circ$ with respect to the ED for crystal III, as demonstrated in Fig. 2c.

The corresponding EBSD images and the misorientation distributions for crystals I, II and III are shown in Figs. 3–5, respectively. Fig. 3a demonstrates the EBSD image of crystal I, and the color lines stand for grain boundaries (GB) with different misorientations. Fig. 3b shows the distribution of the misorientation angles of crystal I after ECAP. It should be pointed out that the GB with misorientation angle smaller than 3° are not shown on the EBSD images. It is found that the microstructures for crystal I after ECAP are large, as observed by SEM-ECC in Fig. 2. All the misorientation angles are $< 15^\circ$. Therefore, after one-pass ECAP crystal I may still be regarded as a single crystal if 15° is considered as a critical value of high-angle GB. The current result is comparable with the report by Miyamoto et al. [22,23], who utilized a series of copper single crystals with similar orientation.

Fig. 4 shows the EBSD image of crystal II and the corresponding misorientation distributions. The grains and

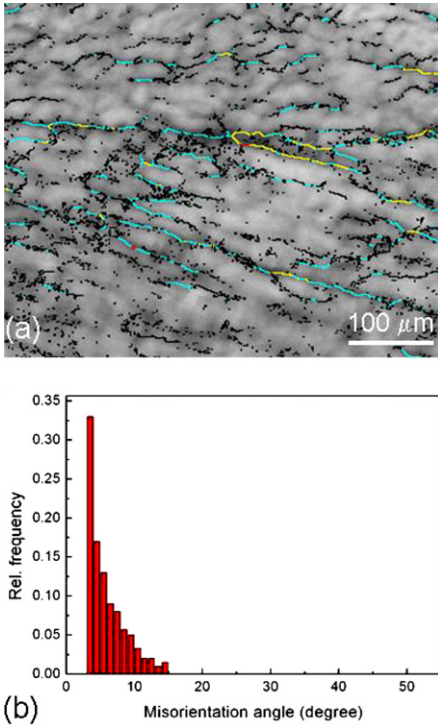


Fig. 3. EBSD micrographs of crystal I: (a) band contrast image combined with GB contours; (b) GB misorientation distribution.

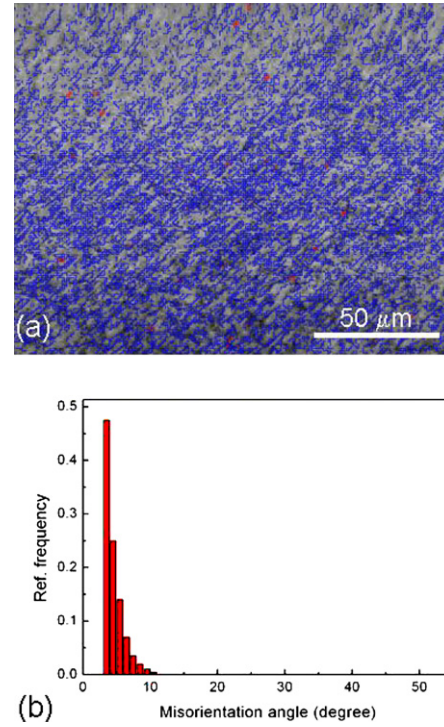


Fig. 5. EBSD micrographs of crystal III: (a) band contrast image combined with GB contours; (b) GB misorientation distribution.

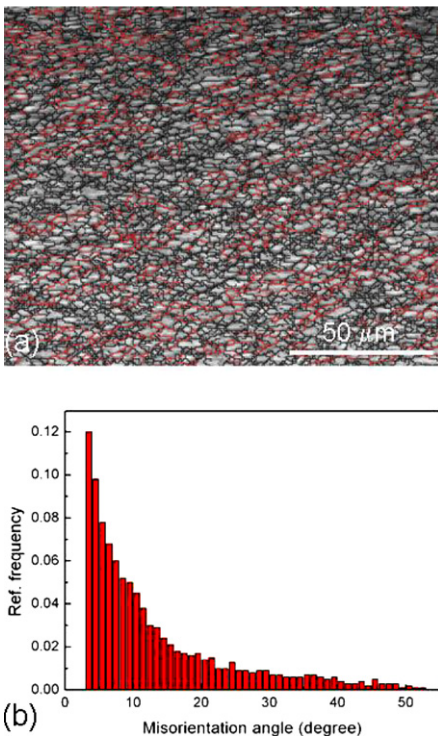


Fig. 4. EBSD micrographs of crystal II: (a) band contrast image combined with GB contours; (b) GB misorientation distribution.

sub-grains are the smallest among the three single crystals and the grain size is on a scale of several microns. The red lines in Fig. 4a stand for the GB with misorientation

angle $>15^\circ$, the corresponding fraction reaches as high as 20%. This demonstrates that the misorientation angles have been significantly increased even by only one-pass ECAP for crystal II, which is different from the misorientation changes for crystal I and crystal III, indicating that crystallographic orientation plays a significantly role in the microstructural refinement and the dislocation structure evolution. The largest misorientation angle for crystal II is $\sim 50^\circ$, which is comparable with the results by Fukuda et al. [20,21].

Fig. 5 demonstrates the EBSD image of crystal III and its GB misorientations. The blue lines on the image stand for the GB with misorientation angles smaller than 10° . It can be clearly observed that those GB get an angle of 45° with respect to the ED, which is the same as the result by SEM-ECC. Most of the GB misorientation angles are smaller than 10° , and only a few parts have larger misorientation. Compared with crystal I, crystal III is closer to a single crystal, because most of the GB misorientations are $<10^\circ$.

The (111) pole figures of the three single crystals before and after ECAP measured by EBSD are shown in Fig. 6. The metal billets have been rotated $\sim 90^\circ$ around the TD during extrusion. Therefore, the pole figures of the deformed crystals have a 90° anti-clockwise rotation compared with the initial pole figures, as shown in Fig. 6. It can be seen that the orientations of the sub-grains in crystal I after ECAP are uniformly scattered around the initial position which reflects a homogeneous distribution of the orientations, while for crystal II, its orientations have been

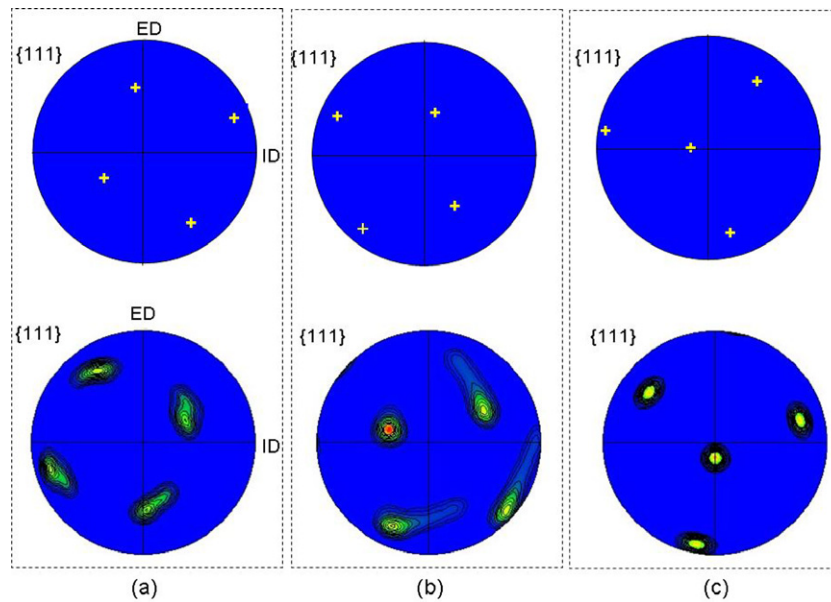


Fig. 6. Pole figures for three single crystals before (upper one) and after (lower one) one-pass ECAP in ID-ED plane: (a) crystal I; (b) crystal II; (c) crystal III.

scattered along certain directions with maximum misorientation $>50^\circ$, indicating a kind of non-uniform deformation, whereas the most special result comes from crystal III: its orientation almost has no scatter, which strongly displays that crystal III still remains single orientation in nature. The above results remarkably demonstrate the significant effects of crystallographic orientation on the microstructural refinement and the dislocation structure evolution during ECAP.

3.2. Microstructures characterized by TEM

The extruded samples were inspected by TEM, with the observations taken on the ID-ED plane at the centre part of the billet. Totally different microstructural features were found in those ECAPed single crystals. Fig. 7a and b presents typical bright-field TEM micrographs of the microstructures and the corresponding selected area diffraction (SAD) patterns of crystal I. After the first pressing, the microstructures in the ID-ED plane mainly consist of cell blocks with approximately square shape divided by two sets of dense dislocation walls perpendicular to each other. As shown in Fig. 7a, most boundaries are sharply delineated, and the contrast across them is small, i.e., these are typical images of sub-boundaries. The existence of sub-grains with small misorientation is also confirmed by the corresponding SAD pattern with almost no scatter. Fig. 7b is a magnification of local microstructures of crystal I. Well-developed sub-grains with curving GB were formed. The SAD patterns and the lower contrast of the bright-field TEM image demonstrate that the misorientation angles between those cell blocks are small, which is well consistent with the observations by EBSD, as shown in Fig. 3.

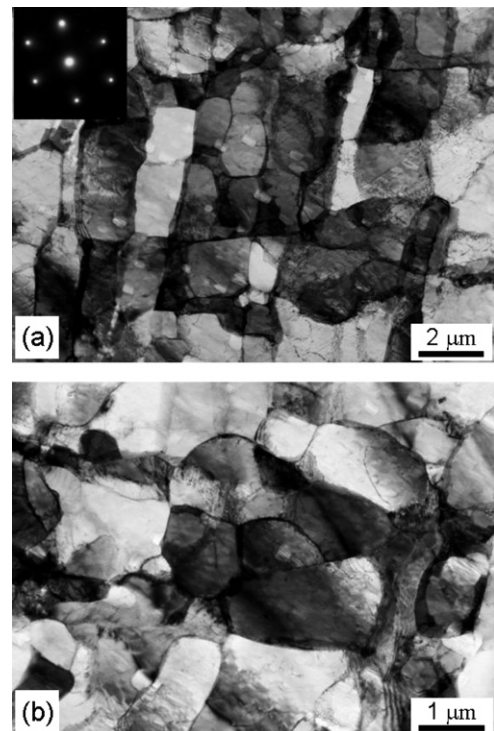


Fig. 7. TEM micrographs of deformation microstructures for crystal I after one-pass ECAP.

Fig. 8 displays the bright-field TEM micrographs of microstructures and the corresponding SAD patterns of crystal II. The characteristic of the microstructures for crystal II is distinct from the cell block microstructures of crystal I. The microstructures for crystal II consist mainly of two sets of sub-grains. The angle between the two directions is $\sim 70^\circ$. This feature is similar to the structures

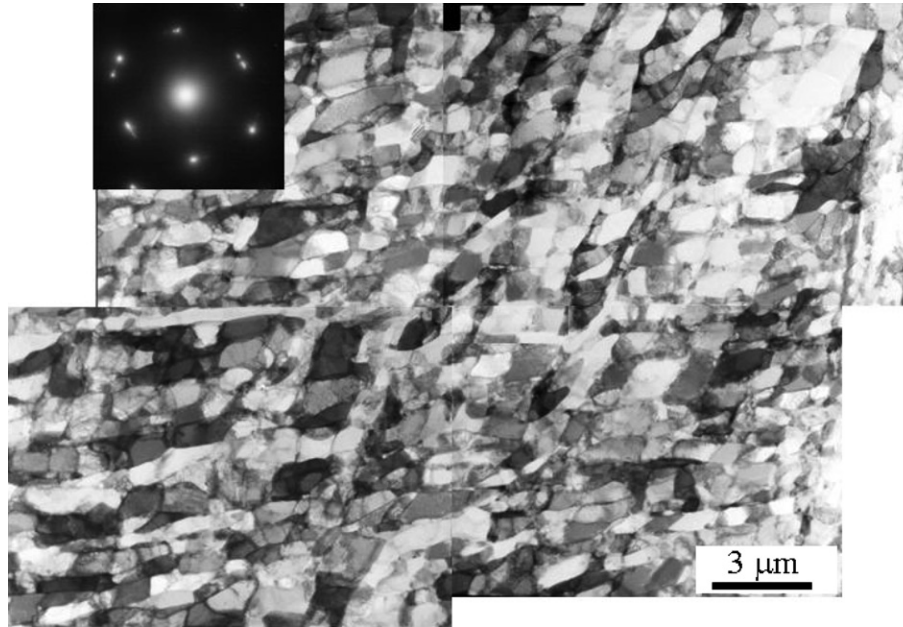


Fig. 8. TEM micrographs of deformation microstructures for crystal II after one-pass ECAP.

observed by Huang et al. [37] and Liu et al. [38]. But the deformation mode and the total strain applied during their experiments are different from the present ECAP process. The SAD patterns are composed of scattered and elongated spots, indicating the average misorientation angle is large for crystal II. The diffraction patterns clearly demonstrate that the two sets of ribbon grain structures are induced by activating two slip planes during ECAP. Fukuda et al. [20,21] also found two types of microstructures in their experiment, labeled A and B, within a single crystal with the same orientation to crystal II, but extruded in a slightly different ECAP die. However, they considered that the formation process of regions A and B were induced by rotating crystallographic orientations. The observations by Fukuda et al. [20,21] are totally different from the present experimental results. Section 4 attempts to give a reasonable explanation for the present observation.

Fig. 9a is a magnification of local microstructures in Fig. 8. Most boundaries with distinct contrast are found to be high-angle ones, while sub-boundaries with low-angle misorientations exist inside some refined grains. The refined grains are further subdivided by the sub-boundaries. Low- to high-angle boundaries are spatially mixed throughout the microstructures owing to the inhomogeneity of deformation, which is similar to Cu after SPD [7]. Fig. 9b presents the microstructures of crystal II close to the lower edge of the ECAPed billet. A clear shear feature can be found in this picture, indicating that there is a remarkable influence of friction on the microstructural formation during ECAP.

Fig. 10 demonstrates the bright-field TEM micrographs of microstructures and the corresponding SAD patterns of crystal III. Its microstructure is characterized by one set of extended dislocation boundaries and is parallel to one slip

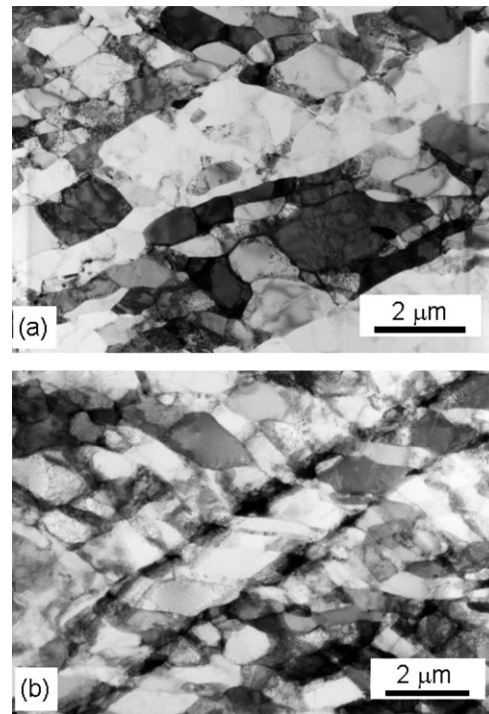


Fig. 9. TEM micrographs of crystal II: (a) a magnification of local image; (b) microstructural image at the lower edge of billet.

plane trace. These parallel boundaries are inclined with respect to the shear direction and separate blocks of ordinary dislocation cells. The SAD patterns clearly show that this kind of ribbon microstructures is the result of activating one primary slip plane during ECAP. Liu et al. [38] and Huang et al. [37] also found similar microstructures in their experiments, and they considered that their crystals have a

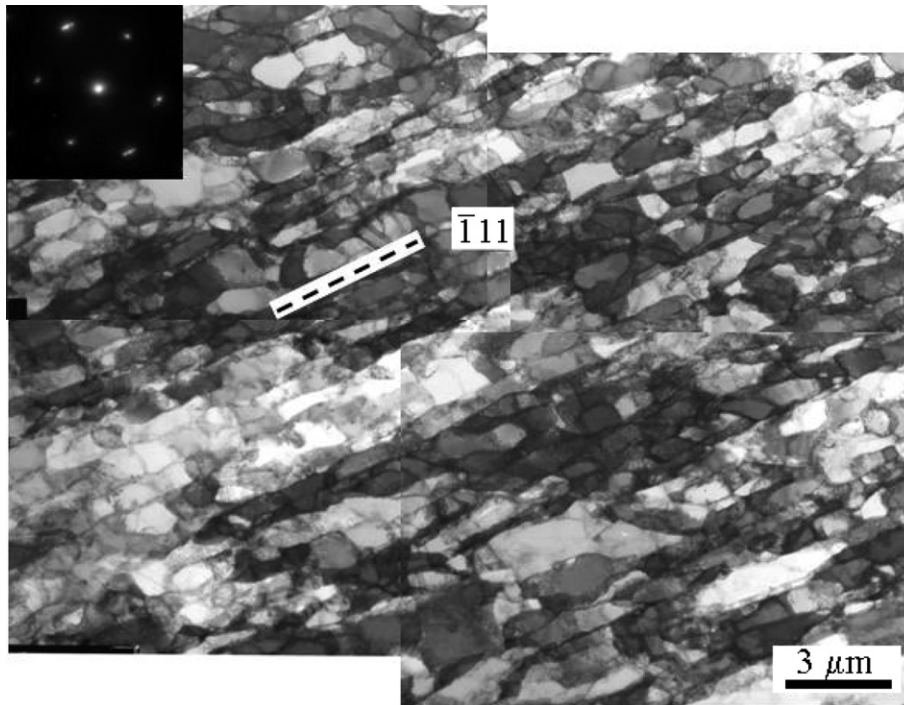


Fig. 10. TEM micrographs of deformation microstructures for crystal III after one-pass ECAP.

tensile axis close to $[1\ 1\ 0]$, whereas the crystals in this investigation were sheared along $[1\ 1\ 0]$ direction during ECAP. A magnification observation reveals that the dense dislocation walls are formed within those ribbon structures, and most boundaries are sharply delineated and the contrast across them is small, as demonstrated in Fig. 11a and b. The TEM observations above clearly display that the crystallographic orientations have a considerable influence on the microstructural evolution during ECAP.

4. Discussion

The results obtained in this investigation provide a clear demonstration of the significant influence of crystallographic orientation on the dislocation structure formation and the misorientation distribution of induced grains and sub-grains in single crystals subjected to ECAP. The different microstructural features for single crystals with different orientations must be induced by the interaction between shear deformation imposed by the ECAP die and the intrinsic slip deformation of those single crystals.

4.1. Definition of shear factor

In order to evaluate the activated slip systems, the magnitudes of the resolved shear stresses and the interaction pattern between ECAP die and single crystals, shear factors were calculated with a similar definition as in Refs. [20,21]. Fig. 12 shows a schematic illustration of the relationship between the slip plane and the slip direction in the single crystals and the relationship between the shear plane and

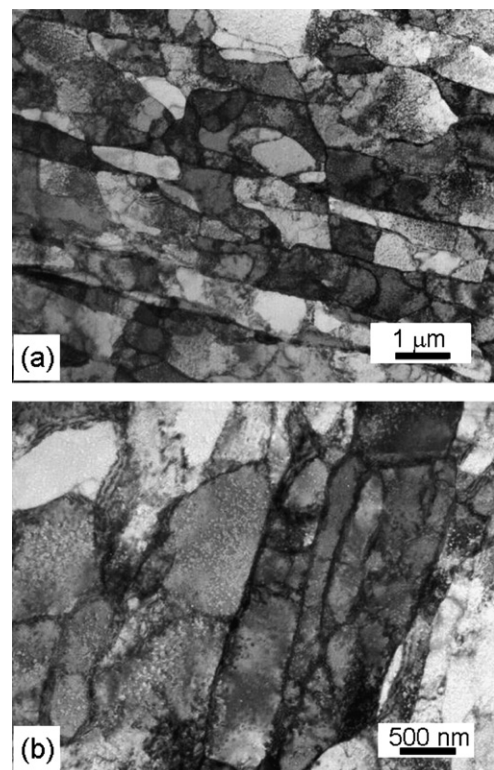


Fig. 11. Magnification TEM micrographs of deformation microstructures for crystal III after one-pass ECAP.

the shear direction in the ECAP die. Noting that the specimen is pressed through the die in a vertical sense, as indicated by the upper vertical arrow in Fig. 12, and defined F

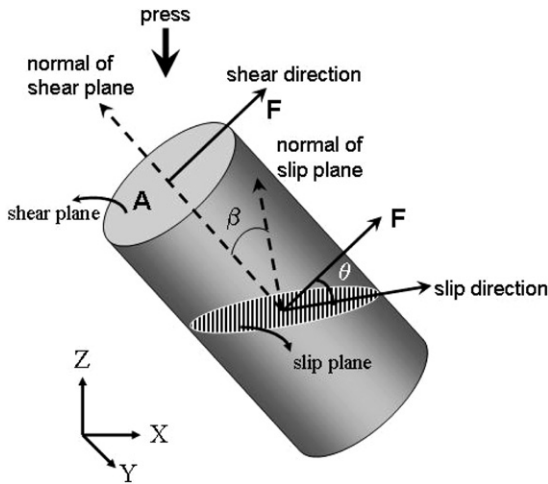


Fig. 12. Schematic illustration of the geometric relations between the resolved shear stresses for a slip system in a single crystal and the shear plane and shear direction in an ECAP die.

as the force in the shear direction and A as the area of the shear plane, it follows that the shear stress τ operating on the slip plane in the slip direction is given by a relationship of the following type for each possible slip system within the three single crystals:

$$\tau = \left(\frac{F}{A}\right) \cos \theta \cos \beta \quad (1)$$

where θ is the angle between the shear direction and the slip direction, and β is the angle between the two normals to the shear and slip planes, respectively. Here, we define the magnitude of the angular term $\omega = \cos \theta \cos \beta$ as shear factor. When considering all the possible slip systems, ω will have values ranging from 0 to 1. It follows, therefore, that the preferential slip system may be predicted by estimating the values of shear factors for all possible slip systems and then selecting the system with the highest value of shear factor.

4.2. The relationship between deformation mode and microstructures

For convenience, let us consider the cases of crystal II and crystal III first. Since the two crystals have the same orientations in nature, their deformation behaviors would have no difference when subjected to uniaxial tensile or compressive loading while, during ECAP, crystal II and crystal III exhibit totally different microstructural features, implying that the ECAP die has a significant constraint effect on the deformation processes of the two single crystals. It is generally considered that the deformation in ECAP is realized through simple shear along the intersection plane [27–29]. Therefore, the values of shear factors for all the slip systems in crystal II and crystal III can be calculated according to the simple shear model and the definition of shear factor above.

For crystal II, the shear plane and the shear direction should be $(\bar{1}11)$ and $[110]$, respectively. The corresponding shear factors for all the slip systems in crystal II are listed in Table 1, where the slip systems with the highest shear factor are in bold. It is apparent that there is only one primary slip system $(\bar{1}11)[110]$ with the highest shear factor of 1.00 for crystal II, while the other three slip planes only have lower shear factor values <0.50 and are hard to be activated during ECAP deformation. Let us have a look at the typical bright-field TEM micrograph of the microstructures of crystal II, as shown in Fig. 13. The crystal II is composed of a cell block with two sets of extended sub-grain structures, which are parallel to the traces of (111) and $(\bar{1}11)$, respectively. This result indicates that there are two primary slip planes activated during ECAP, which is inconsistent with the prediction by simple shear model above [30–32].

For crystal III, in the simple shear model, the shear plane and the shear direction are (110) and $[\bar{1}11]$, respectively. The corresponding shear factors for all the slip sys-

Table 1

The shear factors, and their relevant importance, for various slip systems in crystal II based on the general simple shear theory; the shear plane and the shear direction are $(\bar{1}11)$ and $[110]$, respectively

Slip plane	Slip direction	Shear factor, ν	Order of shear factor
$\bar{1}11$	110	1.00	(1)
	01 $\bar{1}$	0.50	(2)
	101	0.50	(2)
111	011	0.17	(4)
	101	0.17	(4)
	110	0.00	(5)
11 $\bar{1}$	$\bar{1}0\bar{1}$	0.17	(4)
	011	0.17	(4)
	110	0.00	(5)
$\bar{1}1\bar{1}$	110	0.33	(3)
	10 $\bar{1}$	0.17	(4)
	011	0.17	(4)

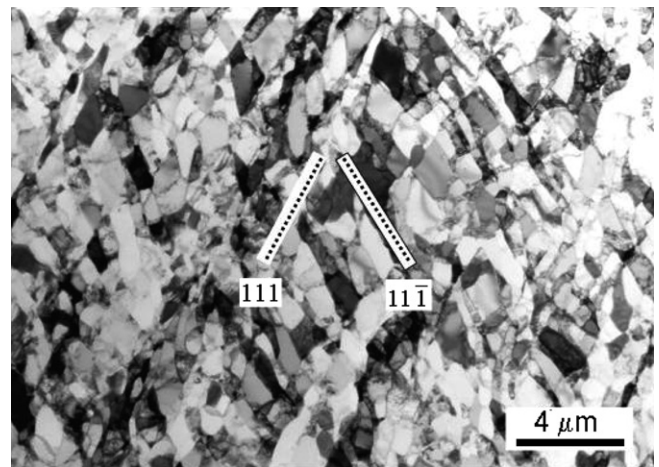


Fig. 13. TEM micrographs of deformation microstructure for crystal II in the central portion of the deformed materials showing the presence of two set of sub-grain structures induced by two primary slip planes activated.

tems in crystal III are listed in Table 2. In this case, there are four slip systems on the (111) or (11 $\bar{1}$) plane with the same shear factor of 0.67; however, the shear factors of the other slip systems are close to zero. This indicates that there are four possible slip systems activated in crystal III during the ECAP deformation, which will result in a complicated microstructure. Fig. 14 shows a typical bright-field TEM image of the microstructures of crystal III. It can be seen that there is only one set of extended dislocation boundaries, which are well developed and parallel to the traces of ($\bar{1}11$). The microstructural features above strongly indicate that there is only one activated primary slip plane in crystal III, which is also contradictory with the prediction by theoretical analysis. It seems that the general understanding of the deformation mode of ECAP cannot well explain the different microstructures in the current single crystals.

Recently, there have been many finite element analyses investigations [39–41] and modeling experiments [35,36]

Table 2

The shear factors, and their relevant importance, for various slip systems in crystal III based on the general simple shear theory; the shear plane and the shear direction are (110) and [$\bar{1}11$], respectively

Slip plane	Slip direction	Shear factor, ν	Order of shear factor
$\bar{1}11$	110	0.00	(2)
	01 $\bar{1}$	0.00	(2)
	$\bar{1}0\bar{1}$	0.00	(2)
111	01 $\bar{1}$	0.00	(2)
	10 $\bar{1}$	0.67	(1)
	$\bar{1}10$	0.67	(1)
11 $\bar{1}$	$\bar{1}0\bar{1}$	0.00	(2)
	011	0.67	(1)
	$\bar{1}10$	0.67	(1)
$\bar{1}1\bar{1}$	110	0.00	(2)
	10 $\bar{1}$	0.00	(2)
	011	0.00	(2)

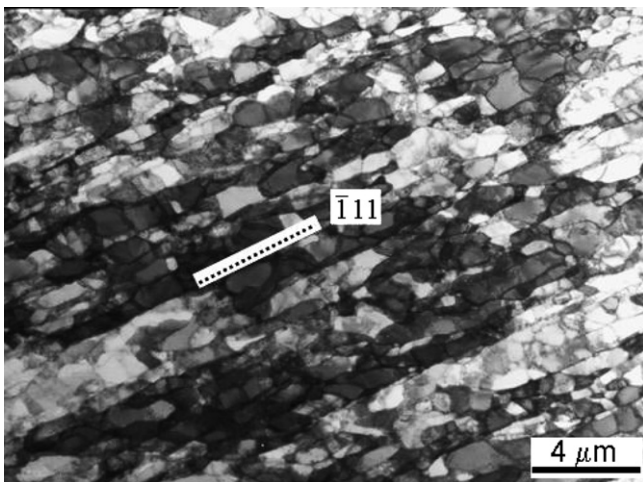


Fig. 14. TEM micrographs of deformation microstructure for crystal III in the central portion of the deformed materials showing the presence of one set of sub-grain structures induced by one primary slip plane activated.

on the deformation mode of ECAP. They considered that the shear deformation may mainly occur along the direction perpendicular to the intersection plane, which is different from the general understanding above. For the right-angle ECAP die, the macro-scale shear deformation may be imposed along the direction vertical to the intersection plane, which is also one of the maximum shear stress directions as pointed out by Segal [28], but no direct experimental evidence can prove this. In the current experiment, crystal III was specially selected to verify this idea. Based on the hypothesis about the deformation mechanism in ECAP and the definition of shear factor above, we recalculated the shear factors of all the slip systems in crystal II and crystal III.

According to the suggested shear direction above, for crystal II, if the corresponding shear plane and shear direction are regarded as (110) and [$\bar{1}11$], respectively, the recalculated shear factors for all the slip systems in crystal II can be found in Table 3. It can be clearly seen that there are two highest shear factors of 0.67 on the two primary slip planes (111) and (11 $\bar{1}$), based on the new suggested shear direction. This prediction is well consistent with the experimental observations about the two sets of sub-grain structures parallel to the traces of (111) and (11 $\bar{1}$), as shown in Fig. 13. For crystal III, the shear deformation should occur on ($\bar{1}11$) plane and along [110] direction. The corresponding shear factors for all the slip systems in crystal III are also calculated and listed in Table 4. The results obviously indicate that only one primary slip system was activated during ECAP for crystal III, because there is only one highest shear factor of 1.00. While the other three slip planes have lower shear factor values <0.50 and are hard to activate during ECAP deformation. This prediction is well consistent with the experimental results either, as presented in Fig. 14. Based on the new suggested shear deformation direction, the microstructural features of crystals II and III can be well illustrated. Therefore, the suggestion about the shear deformation occurring along the direction perpendicular to the intersection plane should be more reasonable than the simple shear theory [27–29].

Table 3

The shear factors, and their relevant importance, for various slip systems in crystal II based on the new suggested shear direction; the shear plane and the shear direction are (110) and [$\bar{1}11$], respectively

Slip plane	Slip direction	Shear factor, ν	Order of shear factor
$\bar{1}11$	110	0.00	(2)
	01 $\bar{1}$	0.00	(2)
	$\bar{1}0\bar{1}$	0.00	(2)
111	01 $\bar{1}$	0.00	(2)
	10 $\bar{1}$	0.67	(1)
	$\bar{1}10$	0.67	(1)
11 $\bar{1}$	$\bar{1}0\bar{1}$	0.00	(2)
	011	0.67	(1)
	$\bar{1}10$	0.67	(1)
$\bar{1}1\bar{1}$	110	0.00	(2)
	10 $\bar{1}$	0.00	(2)
	011	0.00	(2)

Table 4
The shear factors, and their relevant importance, for various slip systems in crystal III based on the new suggested shear direction; the shear plane and the shear direction are $\bar{1}11$ and $[110]$, respectively

Slip plane	Slip direction	Shear factor, v	Order of shear factor
$\bar{1}11$	110	1.00	(1)
	01 $\bar{1}$	0.50	(2)
	$\bar{1}0\bar{1}$	0.50	(2)
111	01 $\bar{1}$	0.17	(4)
	10 $\bar{1}$	0.17	(4)
	$\bar{1}10$	0.00	(5)
11 $\bar{1}$	$\bar{1}0\bar{1}$	0.17	(4)
	011	0.17	(4)
	$\bar{1}10$	0.00	(5)
$\bar{1}\bar{1}\bar{1}$	110	0.33	(3)
	10 $\bar{1}$	0.17	(4)
	011	0.17	(4)

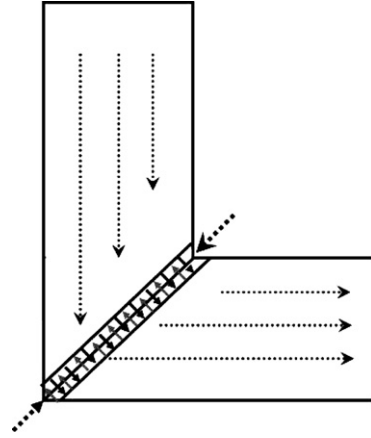


Fig. 15. The illustration of the deformation principle during ECAP for ideal state.

For crystal I, its crystal orientation is very special among the three orientations. For $[110]$ single crystal, its orientation will stay without rotation during uniaxial compression, because this orientation may slip symmetrically on four slip systems from two slip planes [21], and this also can be confirmed by calculation using the shear factor. This symmetrical slip is considered to be the reason that the crystals tend to form the homogeneous deformation microstructure and have a very low shear banding tendency, while crystal I not only has an insert direction parallel to $[110]$, but also has ED parallel to $[\bar{1}11]$. On one hand, this orientation meets the symmetrical slip; on the other hand, the special selected ED also satisfies the shear deformation during ECAP to some extent. For these two reasons, the microstructures for crystal I will stay homogeneous and have relatively low misorientation as shown in Figs. 2a, 3 and 6.

4.3. Deformation mode in ECAP

The specially designed experiments described above obviously indicate that the microstructural features of the three single crystals are not well explained by the simple shear theory [27–29], while the new suggested deformation mode can give a more reasonable explanation. Previous

studies [35,36,39–41] have demonstrated that deformation takes place only near the intersection plane for the ideal case or within a deformation zone for the real case. The single crystal experiments above displayed that the macro-scale shear deformation actually occurs along the direction vertical to the intersection plane, which is the same direction as the tangent of the flow lines [36], rather than the general considered shear deformation along the intersection direction. Based on the analysis above, a possible deformation mode during ECAP is proposed for the ideal case, as shown in Fig. 15. The material will undergo SPD at the adjacent region of the intersection plane, while the macro-scale shear deformation direction is vertical to the intersection plane.

As demonstrated in Fig. 2, for crystal III, a set of ribbon structures with an angle of $\sim 45^\circ$ with respect to the ED were formed after one-pass ECAP. Those ribbon structures are different from the shear flow lines formed within polycrystalline materials after ECAP, which makes an angle of $\sim 27^\circ$ with respect to the ED [30–35]. The formation mechanism of those ribbon structures in crystal III is illustrated schematically in Fig. 16. The ECAP process can be considered as a combination of simple shear perpendicular to the intersection plane and bending imposed by the ECAP die.

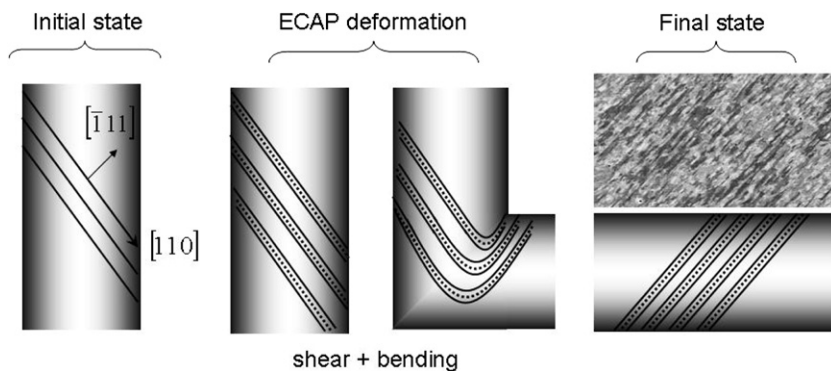


Fig. 16. Illustration of the formation process of 45° ribbon structures for crystal III after one-pass ECAP. The ECAP process can be considered as the combined deformation of simple shear and bending.

For crystal III, the initial shear deformation occurs along the (111) plane and forms a set of extended dislocation structures. After that, the whole billet has a 90° rotation around the TD, which was realized through gradually bending deformation. In this case, it is not difficult to understand why those ribbon structures make an angle of ~45° with respect to the ED in the final state, as illustrated in Fig. 16. Therefore, the shear stress along the intersection plane makes the metal billet rotate during deformation, whereas the shear stress perpendicular to the intersection plane leads to the shear deformation.

In summary, crystallographic orientation has a remarkable influence on the dislocation structure evolution of different single crystals during ECAP. The new suggested shear deformation mode in ECAP can well illustrate the microstructural evolution of the three Al single crystals in the present study. According to the deformation process of crystal III, one finds that the ECAP process could be considered as a special one-dimension deformation for simplicity, which is a unique feature of the ECAP deformation. Furthermore, the present results may be beneficial to the optimum properties of the ECAPed materials and the understanding of the texture evolution during ECAP as well as the application of ECAP technique.

5. Conclusions

Three Al single crystals with different orientations were subjected to ECAP for one-pass. The microstructural evolution and the orientation changes were characterized by various techniques. Based on the experimental observations and the analysis, the following conclusions can be drawn.

- (1) Crystallographic orientations have a remarkable influence on the microstructural evolution of the single crystals subjected to ECAP. For crystal I, there are some cell block structures with multi-slip characters induced by slip symmetrically on four slip systems. In crystal II, two sets of sub-grain structures with high misorientation are formed and make an angle of ~70° because of two asymmetric primary slip planes activated simultaneously. For crystal III, there is only one set of ribbon structures parallel to the traces of ($\bar{1}11$) with lowest misorientation angle among the three single crystals, induced by the homogenous slip on one primary slip plane.
- (2) It is suggested that the macro-scale shear deformation during ECAP occurs along the direction vertical to the intersection plane, which is different from the general simple shear theory. There are two maximum shear stresses during ECAP. However, they play a different role in the shear deformation. The shear stress along the intersection plane makes the metal billet rotate with a local bending during deformation; whereas the shear stress perpendicular to the intersection plane leads to the shear deformation of the metal

billet. The process of ECAP can be considered as a combined deformation of simple shear and local bending.

Acknowledgements

The authors thank Ms. Zhang MJ for her assistance in the TEM experiments. This work was financially supported by National Natural Science Foundation of China (NSFC) under Grant Nos. 50471082, 50371090 and 50571102. Zhang ZF acknowledge the financial support of the ‘Hundred of Talents Project’ by the Chinese Academy of Sciences and the National Outstanding Young Scientist Foundation under Grant No. 50625103.

References

- [1] Hansen N. *Metall Mater Trans A* 2001;32:2917–35.
- [2] Ueji R, Tsuji N, Minamino Y, Koizumi Y. *Acta Mater* 2002;50:4177–89.
- [3] Valiev RZ, Islamgaliev RK, Alexandrov IV. *Prog Mater Sci* 2000;45:103–89.
- [4] Valiev RZ, Langdon TG. *Prog Mater Sci* 2006;51:881–981.
- [5] Lu K, Lu J. *Mater Sci Eng A* 2004;375:38–45.
- [6] Lowe TC, Valiev RZ, editors. *Investigations and applications of severe plastic deformation*. Dordrecht: Kluwer Academic Publishers; 2000.
- [7] Huang CX, Wang K, Wu SD, Zhang ZF, Li GY, Li SX. *Acta Mater* 2006;54:655–65.
- [8] Li SY, Beyerlein IJ, Necker CT. *Acta Mater* 2006;54:1397–408.
- [9] Li SY, Beyerlein IJ, Necker CT, Alexander DJ, Bourke M. *Acta Mater* 2004;52:4859–75.
- [10] Toth LS, Massion RA, Germain L, Baik SC, Suwas S. *Acta Mater* 2004;52:1885–98.
- [11] Gholinia A, Bate P, Prangnell PB. *Acta Mater* 2002;50:2121–36.
- [12] Iwahashi Y, Horita Z, Nemoto M, Langdon TG. *Acta Mater* 1997;45:4711–33.
- [13] Iwahashi Y, Horita Z, Nemoto M, Langdon TG. *Acta Mater* 1998;46:3317–31.
- [14] Neishi K, Horita Z, Langdon TG. *Mater Sci Eng A* 2002;325: 54–8.
- [15] Dalla Torre F, Lapovok R, Sandlin J, Thomson PE, Davies CHJ, Pereloma EV. *Acta Mater* 2004;52:4819–32.
- [16] Komura S, Horita Z, Nemoto M, Langdon TG. *J Mater Res* 1999;14:4044–50.
- [17] Han JH, Oh KH, Lee JC. *Metall Mater Trans A* 2003;34:1675–81.
- [18] Han JH, Suh JY, Oh KH, Lee JC. *Acta Mater* 2004;52:4907–18.
- [19] Li SY, Beyerlein IJ, Alexander DJ, Vogel SC. *Scripta Mater* 2005;52:1099–104.
- [20] Fukuda Y, Oh-ishi K, Furukawa M, Horita Z, Langdon TG. *Acta Mater* 2004;52:1387–95.
- [21] Fukuda Y, Oh-ishi K, Furukawa M, Horita Z, Langdon TG. *Mater Sci Eng A* 2006;420:79–86.
- [22] Miyamoto H, Erb U, Koyama T, Mimaki T, Vinogradov A, Hashimoto S. *Philos Mag Lett* 2004;84:235–43.
- [23] Miyamoto H, Fushimi J, Mimaki T, Vinogradov A, Hashimoto S. *Mater Sci Eng A* 2005;405:221–32.
- [24] Liu Q, Hansen N. *Phys Status Solidi A* 1995;149:187–99.
- [25] Hansen N, Huang X. *Acta Mater* 1998;46:1827–36.
- [26] Wert JA, Liu Q, Hansen N. *Acta Metall Mater* 1995;43:4153–63.
- [27] Segal VM. *Mater Sci Eng A* 1995;197:157–64.
- [28] Segal VM. *Mater Sci Eng A* 1999;271:322–33.
- [29] Segal VM. *Mater Sci Eng A* 2003;345:36–46.

- [30] Fang DR, Zhang ZF, Wu SD, Huang CX, Zhang H, Li JJ, et al. *Mater Sci Eng A* 2006;426:305–13.
- [31] Han WZ, Zhang ZF, Wu SD, Li SX, Wang YD. *Philos Mag Lett* 2006;86:435–41.
- [32] Han WZ, Zhang ZF, Wu SD, Li SX. *Philos Mag Lett* 2007;87:781–8.
- [33] Han BQ, Lavernia EJ, Mohamed FA. *Metall Mater Trans A* 2003;34:71–83.
- [34] Kamachi M, Furukawa M, Horita Z, Langdon TG. *Mater Sci Eng A* 2003;347:223–30.
- [35] Shan AD, Moon IG, Ko HS, Park JW. *Scripta Mater* 1999;41:353–7.
- [36] Han WZ, Zhang ZF, Wu SD, Li SX. *Mater Sci Eng A*; in press.
- [37] Huang X, Borrego A, Pantleon W. *Mater Sci Eng A* 2006;319:237–41.
- [38] Liu Q, Jensen DJ, Hansen N. *Acta Mater* 1998;46:5819–38.
- [39] Semiatin SL, Delo DP, Shell EB. *Acta Mater* 2000;48:1841–51.
- [40] Kim HS, Seo MH, Hong SI. *J Mater Proc Tech* 2002;130:497–503.
- [41] Li SY, Bourke MAM, Beyerlein IJ, Alexander DJ, Clausen B. *Mater Sci Eng A* 2004;382:217–36.